Toward an Understanding of the Microstructure and Interfacial Properties of PIMs/ZIF-8 Mixed Matrix Membranes

Towards an understanding of the microstructure and interfacial properties of PIMs/ZIF-8 mixed matrix membranes.

Marvin Benzaqui,[‡] Rocio Semino,[ζ] Nicolas Menguy,[⊥] Florent Carn,[ϕ] Tanay Kundu,[‡] Jean-Michel Guigner, [⊥] Neil B. McKeown,[§] Kadhum J. Msayib, [§] Mariolino Carta, [§] Richard Malpass-Evans,[§] Clément Le Guillouzer,[φ] Guillaume Clet,[φ] Naseem A. Ramsahye[ζ] Christian Serre,[‡] Guillaume Maurin,[ζ] Nathalie Steunou[‡,*]

[‡]Institut Lavoisier de Versailles, UMR CNRS 8180, Université de Versailles St Quentin en Yvelines, Université Paris Saclay, 45 avenue des Etats-Unis 78035 Versailles Cedex. France**.**

[ζ] Institut Charles Gerhardt Montpellier UMR 5253 CNRS, Université de Montpellier, Place E. Bataillon, 34095 Montpellier Cedex 05, France

[⊥] Institut de Minéralogie de Physique des Matériaux et de Cosmochimie, UMR 7590 CNRS UPMC Univ Paris 06 MNHN IRD – Sorbonne Universités, 4 place jussieu, 75252 Paris cedex 05, France.

[ϕ] Laboratoire Matière et Systèmes Complexes (MSC), UMR CNRS 7057, Université Paris Diderot, Bât. Condorcet, 10 rue A. Domon et L. Duquet, 75013 Paris, France.

[§] EastChem School of Chemistry, University of Edinburgh, Joseph Black Building, David Brewster Road, Edinburgh EH9 3JF, U. K.

[φ] Normandie Univ, ENSICAEN, UNICAEN, CNRS, Laboratoire Catalyse et Spectrochimie, 14000 Caen, France.

ABSTRACT

A study integrating advanced experimental and modeling tools was undertaken to characterize the microstructural and interfacial properties of mixed matrix membranes (MMMs) composed of the zeolitic imidazolate framework ZIF-8 nanoparticles (NPs) and two polymers of intrinsic microporosity (PIM-1 and PIM-EA-TB). Analysis probed both the initial ZIF-8/PIM-1 colloidal suspensions and the

final hybrid membranes. By combining dynamic light scattering (DLS), transmission electron microscopy (TEM) analytical and imaging techniques with small-angle X-ray scattering (SAXS), the colloidal suspensions were shown to consist mainly of two distinct kinds of particles, namely polymer aggregates of about 200 nm in diameter and densely packed ZIF-8-NP aggregates of a few 100 nm in diameter with a 3 nm thick polymer top-layer. Such aggregates are likely to impart the granular texture of ZIF-8/PIMs MMMs as shown by SEM-XEDS analysis. At the molecular scale, modeling studies showed that the surface coverage of ZIF-8 NPs by both polymers appears not to be optimal with the presence of micro-voids at the interfaces that indicates only a moderate compatibility between the polymer and ZIF-8. This study shows that the microstructure of MMMs results from a complex interplay between the ZIF-8/PIM compatibility, solvent, surface chemistry of the ZIF-8 NPs and the physico-chemical properties of the polymers such as molecular structure and rigidity.

Keywords: MOF/polymer interface, mixed matrix membrane, Transmission Electron Microscopy, molecular modeling, polymer of intrinsic microporosity, ZIF-8.

■ INTRODUCTION

Polymer membranes for gas separation have been commercialized for more than 30 years for processes such as the production of nitrogen or oxygen from air, natural gas purification or the removal of carbon dioxide from natural gas.[1] They have emerged as a competitive technology owing to their low capital and operating cost, small footprints and ease of operation. However, polymer membranes suffer from a trade-off between permeability and selectivity which is defined by the so-called Robeson upper bound for the specific gas pair of interest.[2,3] Recently, polymers of intrinsic microporosity (PIMs) have attracted great interest for use as gas separation membranes not only due to their promising performances but also to their processability from solution.[4] The molecular structure of PIMs consists of aromatic rings connected by spiro-centers leading to a contorted backbone. The permanent

microporosity and high free volume of PIMs are derived from both low segmental mobility and the sites of contortion that frustrate the packing of polymer chains.[4,5] As a consequence, PIMs possess high gas and vapor permeability as well as good selectivity, surpassing the Robeson upper bound for several gas pairs of technological relevance (i.e. O_2/N_2, CO_2/CH_4, CO_2/N_2).[4,6,7,8] PIM-1 is the most studied polymer of this group (see Scheme 1) with very promising properties in terms of high gas permeability and large solubility coefficients.[6,7,9] However, in common with other glassy polymers (e.g. poly(trimethylsilyl propyne), PTMSP),[10] the gas permeation properties of PIMs are deeply influenced by their processing history.[7,11] For example, ageing involves the slow densification of chain packing over time and this leads to a decrease of the polymer free volume and gas permeability. In addition, gas permeability is strongly affected by the presence of residual solvent and its nature (water, $CHCl_3$ or alcohols).[7] For example, a PIM-1 film shows a permeability coefficient $P(O_2)$ of 120 Barrer after wetting with water but this increased to 1600 Barrer following immersion of the film in ethanol or methanol.[7] This was explained by the swelling of the polymer facilitated by strong hydrogen bonds between the alcohols and the oxygen atoms of the dioxane ring of PIM-1.[12]

In the continuous quest for novel membrane materials, the design of mixed matrix membranes (MMMs) that combine a polymer matrix and inorganic or hybrid fillers has emerged as a valuable approach to enhance the gas transport properties and improve on the upper bound limitations of pure polymers.[13,14] MMMs have the advantages of coupling the good processability and mechanical properties of polymers with the attractive physico-chemical properties of the fillers (e.g. molecular sieving). Initially, impermeable NPs such as oxides (SiO_2, TiO_2, MgO) were introduced in polymer matrices in order to induce a distortion of chain alignment thereby increasing the free volume and gas permeation parameters.[15,16] More recently, permeable porous NPs (i.e. zeolites, activated carbons, mesoporous silicas…) can perform the same role but also provide additional gas transport channels thereby boosting the performance of membranes for gas separation.[17,18,19,20,21,22] For example, Metal Organic Frameworks (MOFs) bring significant advantages including a high separation performance

owing to their size/shape exclusion or selective adsorption of gas molecules as well as their better compatibility with polymers due to their structural tunability.[13,14,23,24,25,26,27] However, optimal separation enhancement generally requires a high particle content that is likely to increase the cost of the membrane, complicate its processing and adversely affect its mechanical properties or durability.[13,14,28,29] In particular, increasing the particle content in MMMs may prevent the dispersion of the fillers in the polymer matrix and favor their aggregation, especially for polymer-filler combinations with poor interfacial compatibility. As a result of insufficient affinity between polymers and fillers, the creation of interphase defects (macro- or nanovoids) is frequently observed for numbers of MMMs and generates new bypasses around the fillers for gas transport that can reduce the gas selectivity of the membranes.[13,14,23,30,31,32] As a consequence, several approaches for the processing of MMMs have been investigated in order to improve the interactions between polymer and MOFs including priming of filler particles,[21, 33] use of co-solvent,[22] functionalization of polymer[34] or MOF,[35,36,37] controlling evaporation rate of solvents,[35] *in-situ* synthesis of MOF particle[29] etc… However, despite some promising results from a few MOF-based MMMs, the preparation of these composite gas separation membranes with the desired morphology, gas separation properties and mechanical/chemical stability is still challenging and empirically-driven.

In this context, MMMs made from PIM-1 and nanoparticles of the zeolitic imidazolate framework ZIF-8 were recently reported by Bushell *et al*.[38] In addition to its high chemical and thermal stability, ZIF-8 exhibits a microporous hybrid framework (see Scheme 1) with a cavity diameter of 11.6 Å accessible through flexible microporous windows of 3.4 Å. Such a topology is expected to confer to the composite molecular sieving properties and thus enhance the separation of small gas molecules from larger ones.[39,40,41] ZIF-8/PIM-1 MMMs do provide data that lie above the 2008 upper bound for several gas pairs.[38] However, other factors such as the nature of the interface between the polymer and the filler as well as the impact of the filler on the chain packing may play a significant role in the gas separation performance of this

composite. Recently, a computational methodology based on a combination of quantum and force-field based-simulations was developed by some of the present authors to characterize the ZIF-8/PIM-1 interface at the atomistic level.[42] Thermodynamically favorable interactions between the –CN groups in PIM-1 and the NH functions at the MOF surface were predicted, although this did not prevent the formation of well-defined microvoids at the interface.

We report here a further investigation of the microstructure and interfacial properties of ZIF-8/PIM-1 MMMs by coupling multiple characterization tools and molecular simulations. As reported previously,[38] a granular texture of the internal surface of ZIF-8/PIM-1 MMMs was clearly evidenced by SEM. However, as no microstructural characterization of the ZIF-8/PIM-1 aggregates was undertaken, it was not possible to unravel a possible relationship between the microstructure of MMMs and their gas transport properties. In the present article, we focus our attention on both the initial ZIF-8/PIM-1 colloidal suspensions and the final hybrid membranes. It is demonstrated that the homogeneity and texture of MMMs, as well as the nature of the PIM-1/ZIF-8 interface, strongly depend on the history of MMM processing and thus on the chemical interactions between ZIF-8 NPs and PIM-1 chains occurring in solution. By coupling TEM analytical and imaging techniques, DLS and SAXS, it is possible to provide a clear picture of the ZIF8-PIMs colloidal solution, which consists mainly of aggregates of a few 100 nm in diameter composed of a core with densely packed ZIF-8 NPs and a polymer shell of about 3 nm thick, in addition to polymer aggregates of about 200 nm in size. The influence of several physico-chemical parameters (e.g. concentration of ZIF-8 NPs, ZIF-8/PIM-1 weight ratio, time of mixing, ultra-sonication) on the structure of these aggregates and the colloidal stability of the ZIF-8/PIM-1 suspensions was investigated. It is shown that the nature and morphology of these hybrid colloids result from a subtle interplay between the affinity of both components and their solubility in the solvent. Finally, PIM-EA-TB[43] (see Scheme 1) was considered as a possible alternative polymer matrix for the preparation of MMMs. By coupling HRTEM and molecular modeling, insight into the surface interactions of ZIF-8 with PIM-EA-TB chains was obtained, thereby enabling us to compare the

interfacial properties of ZIF-8/PIM-1 and ZIF-8/PIM-EA-TB in terms of the nature of the interactions, surface coverage and conformation of the polymer chains. To the best of our knowledge, this is the first time that such a thorough characterization of the interfaces of MOF/polymer composites is reported.

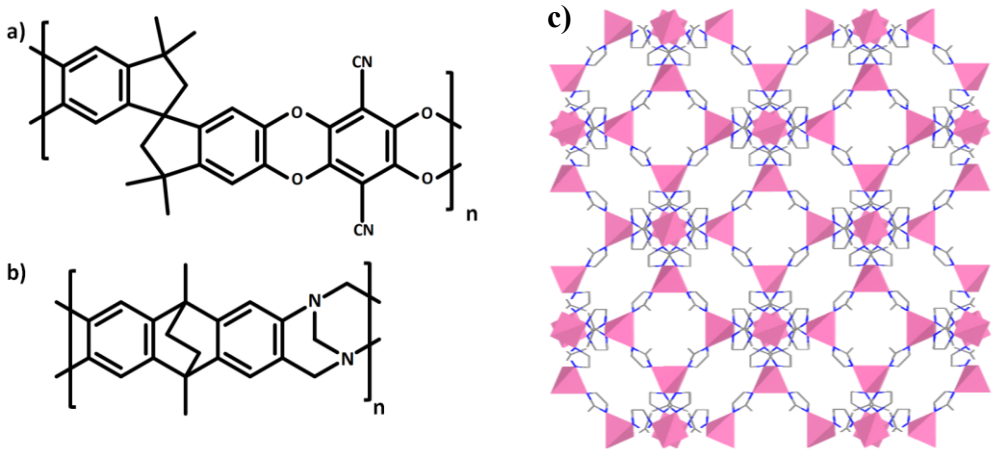

Scheme 1. Molecular structure of (a) PIM-1, (b) PIM-EA-TB and (c) ZIF-8. Zn tetrahedral, carbon and nitrogen atoms are in purple, grey and blue, respectively.

■ EXPERIMENTAL SECTION

Chemicals. $Zn(NO_3)_3$•$6H_2O$ (99%) was purchased from Sigma Aldrich and 2-methylimidazole (Hmim) (97 %) from Alfa Aesar. All chemicals were used as received without further purification.

Synthesis of ZIF-8 nanoparticles. ZIF-8 NPs were synthesized as previously reported by Cravillon *et al.*[44,45] A solution of Hmim (6.489 g, 79.04 mmol) in 200 mL of MeOH was poured into a solution of $Zn(NO_3)_3$•$6H_2O$ (2.933 g, 9.87 mmol) in 200 mL of MeOH at room temperature under stirring. After 1h, the milky solution was centrifuged at 14500 rpm for 15 min to recover ZIF-8 NPs which were then re-dispersed in 30 mL of absolute ethanol and centrifuged again twice to remove the excess of unreacted Hmim and zinc nitrate. The ZIF-8 NPs were washed once again with 30 mL of THF. After final centrifugation, ZIF-8 NPs were re-dispersed and then stored in THF. ZIF-8 NPs were dried overnight at 100°C for further characterization by X-ray powder diffraction (XRPD), thermogravimetric analyses (TGA) and FT-IR spectroscopy.

Preparation of ZIF-8/PIMs membranes. ZIF-8 solutions at concentration of 10 g L^{-1} in THF were obtained by diluting a 15 g L^{-1} stock solution followed by ultra-sonication using a US horn (40%, 1 min). Polymer (i. e. PIM-1 or PIM-EA-TB) was added to the ZIF-8 solution directly as a powder or alternatively as a solution in THF (PIM-1) or $CHCl_3$ (PIM-EA-TB). Solutions of PIM/ZIF-8 mixtures were prepared with different PIM/ZIF-8 weight ratio (90:10, 80:20 and 60:40). After stirring overnight, the PIM/ZIF-8 solutions were cast on a clean Petri dish or sonicated (horn, 10% power) at room temperature for about 1 min before casting. The evaporation of THF was controlled using a funnel.

Preparation of ZIF-8/PIMs colloidal dispersions. ZIF-8 solutions at [ZIF-8] concentrations ranging from 0.01 to 1 g L^{-1} were prepared by diluting an initial 15 g L^{-1} stock solution with THF. ZIF-8 solutions were sonicated using a horn (40% power, 1 min), before adding the polymers (i. e. PIM-1 and PIM-EA-TB) directly as powder or as a solution in THF (PIM-1) or $CHCl_3$ (PIM-EA-TB). Colloidal dispersions of ZIF-8/PIMs with ZIF-8/PIMs weight ratio ranging from 0.1 to 0.7 were prepared. Before DLS measurements, each solution is stirred for 0 to 24 h and eventually sonicated (horn, 10% power, 1 min). For some TEM experiments, the excess of polymer was removed by centrifugation at 14500 rpm for 15 min, followed by the re-dispersion of the solid in THF (PIM-1) and THF/$CHCl_3$ (PIM-EA-TB).

Characterization of ZIF-8/PIMs membranes. The solids were analyzed by FTIR (Nicolet 6700 FTIR spectrometer equipped with a DTGS detector) as self-supported wafers (ca. 15 mg). Spectra of the samples were recorded after heating at 200 °C for 5 hours under secondary vacuum (~10^{-3} Pa). X-ray powder diffraction patterns (XRPD) were collected using Siemens D5000 diffractometer (θ−2θ) with Cu radiation (λK_α = 1.54059 Å). BET surface areas of the materials were determined by N_2 adsorption in a BELSORP-Max porosimeter at 77 K. Prior to the analysis, ZIF-8 NPs were outgassed overnight under dynamic vacuum at 120 °C. Thermogravimetric analyses (TGA) were performed on a Perkins Elmer SDA 6000 apparatus. Solids were heated up to 800 °C with a heating rate of 3 °C.min^{-1} in an oxygen atmosphere. SEM images have been recorded on a JEOL JSM-7001F microscope using gold-

coated samples equipped with an X-ray energy-dispersive spectrometry (XEDS) detector with a X-Max SDD (Silicon Drift Detector) by Oxford.

Characterization of ZIF-8/PIMs colloidal dispersions. Dynamic light scattering (DLS) measurements were performed on a Zetasizer from Malvern Instruments. ZIF-8 and ZIF-8/PIMs solutions with [ZIF-8] = 0.01 to 1 g L^{-1} were sonicated before DLS measurements. Solutions were analyzed in a glass cuvette with a 4 mW HeNe LASER operating at λ = 632.8 nm and a detection angle of 173°. The colloidal stability of ZIF-8/PIMs solutions was evaluated by measuring the evolution of the diameter of particles and polydispersity index (PDI) with time up to a total time of 9 minutes. The integration time per measurement point was 10 seconds. HRTEM images were recorded on a JEOL 2100F microscope operating at 200 kV, equipped with a Schottky emission gun, a high resolution UHR pole piece and a Gatan US4000 CCD camera. Samples were prepared by deposition of one droplet of colloidal suspensions onto a carbon-coated copper grid and left to dry in air. High angle annular dark field in the scanning transmission electron microscopy mode (i.e. STEM-HAADF) experiments were recorded using a JEOL annular detector. In the same way, chemical maps were recorded using a JEOL X-ray energy dispersive spectrometer coupled with the STEM mode (i.e. STEM-XEDS). Small angle X-ray scattering (SAXS) experiments were performed at 25 °C with samples placed in sealed quartz capillaries on SWING beamline (SOLEIL synchrotron at Saint-Aubin, France) with two configurations: (1) D = 2.1 m and λ = 1 Å to get a q-range from 4.8×10^{-3} $Å^{-1}$ to 0.52 $Å^{-1}$ and (2) D = 6 m and λ = 1 Å to get a q-range from 1.5×10^{-3} $Å^{-1}$ to 0.18 $Å^{-1}$

Molecular Modeling. The ZIF-8/PIM-EA-TB interface was modeled by applying the computational strategy based on integrating quantum and force-field based molecular simulation tools, developed recently and applied to the case of the ZIF-8/PIM-1 system.[42] ZIF-8 was described by a slab model of the [011] surface that was previously shown as the lowest energy surface for this MOF. This modeled surface consists of exposed OH groups and imidazole moieties capping the metal atoms at the surface. Moreover, our ZIF-8 model is a collection of fixed atoms, since flexibility has not been found to change

the structure of the ZIF-8/PIM-1 interface.[42] Regarding PIM-EA-TB, a model consisting of 9 polymer chains containing 10-20 monomers each, with a total of 112 monomers, was constructed using the *Polymatic* code.[46] To be consistent with our previous ZIF-8/PIM-1 simulations, this polymer was built in a box of dimensions 50 Å x 50 Å x 150 Å, and then two empty boxes were added in the *z* direction, resulting in a box of dimensions 50 Å x 50 Å x 400 Å. The bonded and non-bonded Lennard-Jones potential parameters for PIM-EA-TB were taken from TraPPE potential[47] while the partial charges for each constituting atom were derived from the electrostatic potential fitting ESP method (see SI for details). All these parameters are provided in Table S2 of SI. The construction and the equilibration of the ZIF-8/PIM-EA-TB interface was further achieved by following a three stages procedure involving force field based- molecular dynamics (MD) as it was previously reported for MOF/PIM-1 system.[42] Details of the methodology are provided in SI. Statistics was collected for 10 independent MD runs of 10 ns.

■ RESULTS AND DISCUSSION:

Colloidal solutions of ZIF-8.

ZIF-8 NPs were synthesized at room temperature through the reaction of bridging 2-methylimidazole (Hmim) ligand with $Zn(NO_3)_3.6H_2O$ in methanolic solution, according to the procedure previously reported.[44,45,48] ZIF-8 presents a cubic microporous architecture with a zeolite topology which consists of Zn^{2+} cations connected to bridging imidazolate anions (see Scheme 1). This anhydrous framework can be described by a space-filling packing of regular truncated octahedra that defines pores of 1.1 nm in diameter connected through apertures of flexible windows of ca. 0.34 nm in diameter.[39] ZIF-8 NPs were characterized by combining XRPD, SEM, TEM, N_2 porosimetry, FTIR and TGA (see Figures S1-S4, S9 of SI). XRPD shows the characteristic Bragg peaks of ZIF-8 with a broadening, in agreement with the presence of NPs (Figure S1). Nitrogen sorption experiment measured at 77 K shows a type I isotherm (Figure S3) with a BET area of 1700 $m^2\ g^{-1}$, in good agreement with the value previously

reported.[48] SEM and TEM experiments (Figure S4) show well-defined ZIF-8 nanocrystals of about 35 nm in diameter with a characteristic rhombic dodecahedral shape as previously reported.[44,45] According to DLS measurements (Figure S5) on ZIF-8 colloidal solutions of 0.1 g L^{-1}, particles with an hydrodynamic diameter (D_h) of about 180 nm are detected in THF, showing an aggregation phenomenon of ZIF-8 NPs. This aggregation process is even more pronounced for a larger ZIF-8 concentration (i. e. 1 g L^{-1}) where aggregates with D_h > 2000 nm are detected (Figure S5). This is in excellent agreement with the TEM observations, showing a network of strongly aggregated and inter-connected ZIF-8 NPs in THF (Figure 1 and Figure S4). The SAXS curve of the ZIF-8 solutions (Figure S6) is characterized by two oscillations, at q = 0.021 $Å^{-1}$ and 0.035 $Å^{-1}$, and fits well to the form factor of spheres with a diameter D = 50.0 nm and a log-normal polydispersity (P.D. = 0.10), in agreement with that previously reported for similar ZIF-8 NPs.[44,45,49]

Characterization of PIM-1 and PIM-EA-TB solutions by DLS and TEM.

PIM-1 and PIM-EA-TB, both of approximate average molecular weight M_n = 50000 g mol^{-1} and M_w = 150000 g mol^{-1} were dissolved in THF and $CHCl_3$, respectively. As previously reported, these solvents appear to dissolve completely the polymers leading to homogeneous and clear solutions with the absence of any visible gel formation.[50] However, the complete dissolution of PIM-1 in THF and PIM-EA-TB in $CHCl_3$ is time consuming and requires several steps of polymer addition. Moreover, such homogeneous solutions are obtained only for polymer concentrations lower than 4 g L^{-1}. Analysis of solutions using DLS indicates a partial aggregation of PIM-1 in THF and PIM-EA-TB in $CHCl_3$. For PIM-1 concentration between 0.1 g L^{-1} and 4 g L^{-1}, two populations of aggregates are detected with D_h = 30 nm and 200 nm (Figure S7 of SI). This is fully consistent with TEM images of a PIM-1 coating (obtained by casting a 1g L^{-1} PIM-1 solution in THF) showing the coexistence of a polymer film and spherical aggregates with a diameter between 25 nm to 150 nm (Figure 1 (b)-(c)). At higher PIM-1 concentration (i.e. 10 g L^{-1}), this aggregation phenomenon is even more pronounced leading to a partial

phase separation of the polymer in solution. DLS measurements show the presence of at least five populations of nano- and micrometer-sized aggregates with diameters ranging between 8 nm to 6000 nm (Figure S7 of SI). Similar observations were made for PIM-EA-TB solutions in chloroform (Figure S7).

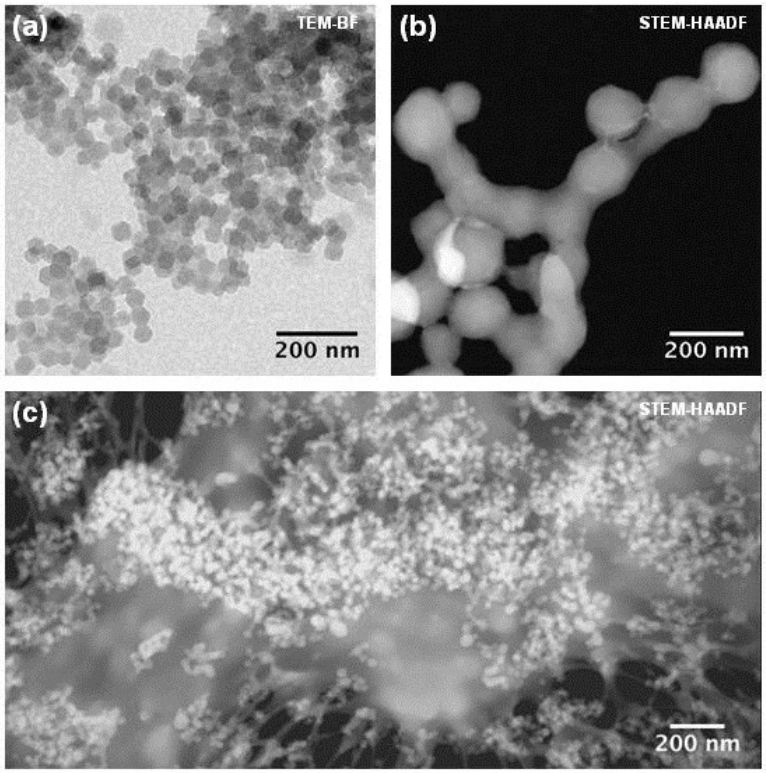

Figure 1: (a) TEM bright field of ZIF-8 NPs in THF and (b-c) STEM-HAADF images of PIM-1 in THF.

ZIF-8/PIM-1 membranes. Self-supported ZIF-8/PIM-1 MMMs (10/90 mass ratio) were prepared by solvent casting. For larger ZIF-8/PIM-1 weight ratios, cracks and fractures are observed in the composites. The XRPD pattern of ZIF-8/PIM-1 membranes presents only the characteristic broad reflections of ZIF-8 NPs (Figure S8 of SI), PIM-1 exhibiting scattering consistent with an amorphous structure. The incorporation of ZIF-8 in PIM-1 is confirmed by FT-IR spectroscopy (Figure S9) showing the characteristic vibration bands of both ZIF-8 NPs and PIM-1. The absence of any shift in the

energy of vibration bands in comparison to those of pure ZIF-8 and PIM-1 suggests a lack of meaningful interactions between ZIF-8 NPs and PIM-1.

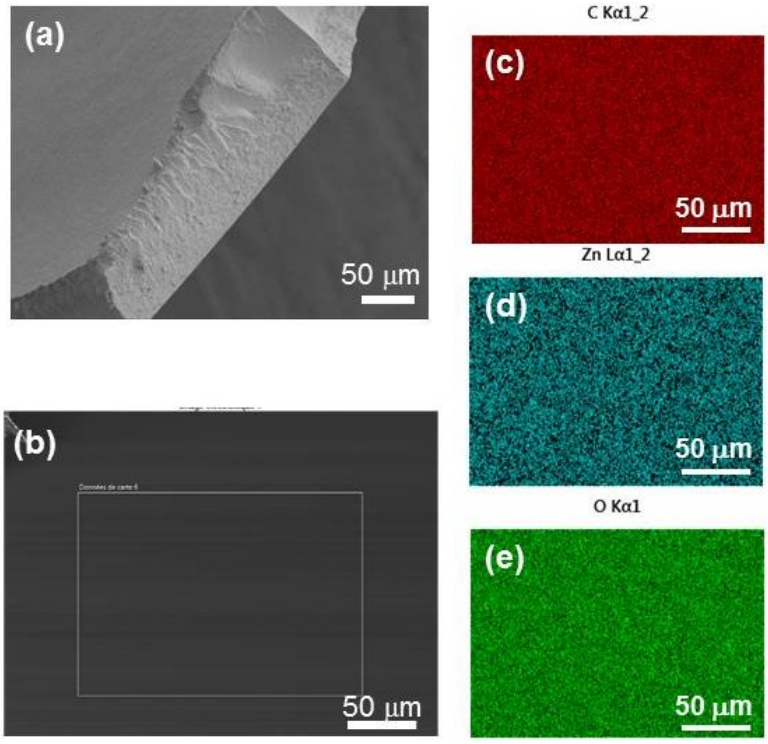

Figure 2. (a-b) SEM images of ZIF-8/PIM-1 membranes (10/90 wt%) and (c-e) elemental mapping of carbon (c), zinc (d) and oxygen (e) by XEDS spectroscopy for the rectangular area indicated by the white box in panel (b).

These results are fully consistent with ^{13}C CP MAS spectra showing the characteristic signals of the pristine ZIF-8 and PIM-1 components with the absence of any shift in ^{13}C chemical shift (Figure S10). As revealed by SEM, the thickness of the supported membranes lies between 70 and 140 µm. For a ZIF-8 content of 10 wt%, flat and homogeneous ZIF-8/PIM-1 membranes were obtained with the absence of aggregates at the surface (Figure 2(a)). The elemental mapping via SEM-XEDS analysis shows a uniform distribution of C, O and Zn elements (Figure 2 (c)-(e)). Noteworthy, these MMMs were obtained from ZIF-8/PIM-1 solutions that were sonicated before solvent casting. In the absence of ultra-sonication, the homogeneity of composites differ significantly since a few ZIF-8 aggregates are clearly

observed by SEM-XEDS mapping (see Figure S11). The non-homogenous distribution of Zn in the section of ZIF-8/PIM-1 composites (i. e. 10 wt % of ZIF-8, ultra-sonication) as shown by SEM-XEDS analysis (see Figure S12 of SI) is indicative of a sedimented layer of ZIF-8 NPs in PIM-1 on the support. This sedimentation presumably takes place between the ultra-sonication step and the evaporation of THF as previously reported for other MMMs.[51,52] This sedimentation process is even more pronounced by increasing the ZIF-8 content to 20 and 40 wt%. SEM images clearly show that the bottom- and top-surfaces of membranes present different microstructural properties (see Figure 3). While an homogeneous and flat top-layer of ZIF-8/PIM-1 (20 wt % of ZIF-8) is observed, their bottom-layer presents a rough and granular texture (Figure 3 (a,b)) which is fully consistent with that previously reported by Bushell *et al.* on ZIF-8/PIM-1 membranes[38] and by Ahn *et al.* on silica/PIM-1 membranes.[16] This granular morphology most probably results from prior aggregation and/or phase separation process taking place in the ZIF-8/PIM-1 mixture. Such results are consistent with the

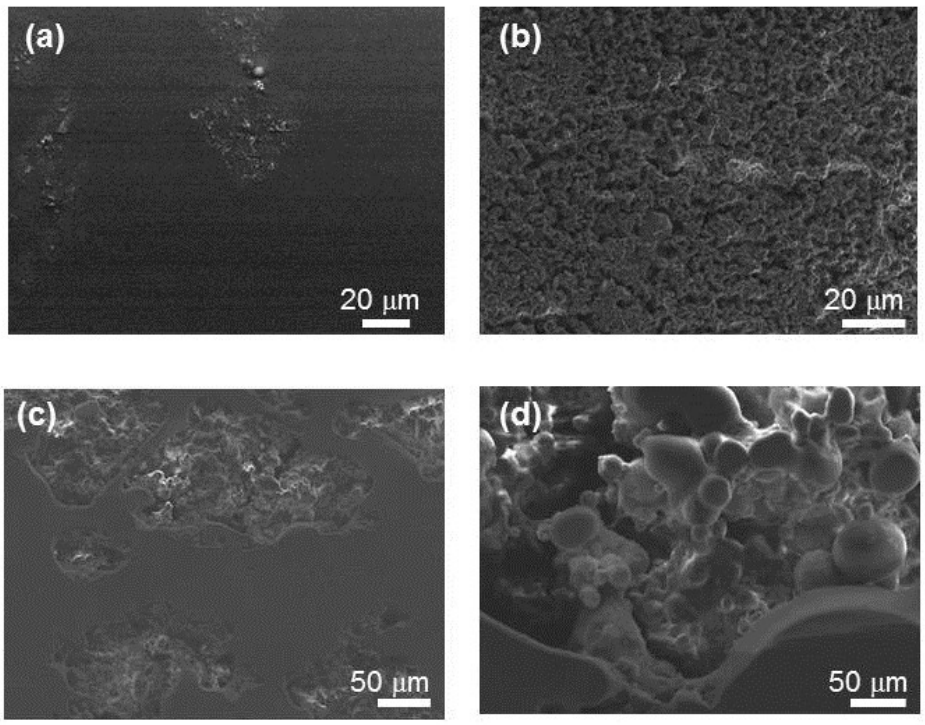

Figure 3. SEM images of ZIF-8/PIM-1 with (a-b) ZIF-8/PIM-1 = 20/80 wt%; and (c-d) 40/60 wt%. (a) and (c) correspond to top-surface of MMMs while (b) and (d) correspond to bottom-surface of MMMs.

elemental mapping via SEM-XEDS analysis, showing an heterogeneous distribution of C, O and Zn elements at the bottom layer of ZIF-8/PIM-1 (20 wt % of ZIF-8) (see Figure S13). Indeed, spherical aggregates of a few hundred nanometers in diameter can be clearly visualized in the structure of ZIF-8/PIM-1 composites for a ZIF-8 content of 40 wt%. (Figure 3 (c)-(d)).

Dilute suspensions of ZIF-8/PIMs.

In order to understand the aggregation phenomenon of ZIF-8 NPs in the presence of PIM-1, the physico-chemical properties of ZIF-8/PIMs solutions were investigated. Unfortunately, casting solutions are too concentrated to be analysed directly by DLS, HRTEM and STEM-HAADF. However, more dilute solutions allow investigation of the aggregation process and interfacial properties between ZIF-8 NPs and polymers that may relevant at higher concentrations. First, ZIF-8/PIM-1 colloidal suspensions (20/80 wt%) in THF with ZIF-8 concentrations of 0.1 and 1 g L^{-1} were studied by combining HRTEM and STEM-HAADF (Figure 4 (a)-(c)) and both suspensions gave similar results. It is noteworthy that two populations of particles were present on the carbon grids – well-defined spherical NPs of 30 nm in diameter together with particles characterized by a larger diameter (100-200 nm) and a high polydispersity in shape ranging from spherical to elongated forms. While the former small NPs may correspond to ZIF-8 NPs, the latter particles can be assigned to PIM-1 aggregates, according to the TEM characterization of pristine ZIF-8 NPs and PIM-1 in THF (see *vide supra*). This assumption was confirmed by STEM-XEDS elemental mapping (see Figure 4(c)). The absence of Zn element in PIM-1 aggregates indicates that no ZIF-8 NPs are incorporated into the polymer particles. On the carbon grid two networks of particles co-exist: a network of strongly aggregated ZIF-8 NPs and another network of inter-connected PIM-1 particles (Figure 4(a)-(c)). Since the TEM observations can be altered by the large amount of polymer, the excess of polymer was removed by centrifugation (see experimental part). As shown by STEM-HAADF (see Figure S14), compact aggregates of a few hundred nanometers in

diameter are observed. This result is in fair agreement with DLS measurements showing the presence of particles with D_h=500 nm after mixing ZIF-8 NPs and PIM-1 for about 24h. These objects consist of an assembly of strongly aggregated ZIF-8 NPs (Figure 5). However, the presence of the polymer at the surface of these aggregates can be clearly visualized by recording HRTEM images and STEM-HAADF (Figure 5 (e-f)). A coating of PIM-1 is present at the surface of ZIF-8 aggregates with a thickness of about 3 nm which is almost constant in the different objects. Apparently, these objects could be described as a "bag" of polymer in which ZIF-8 NPs are closely embedded.

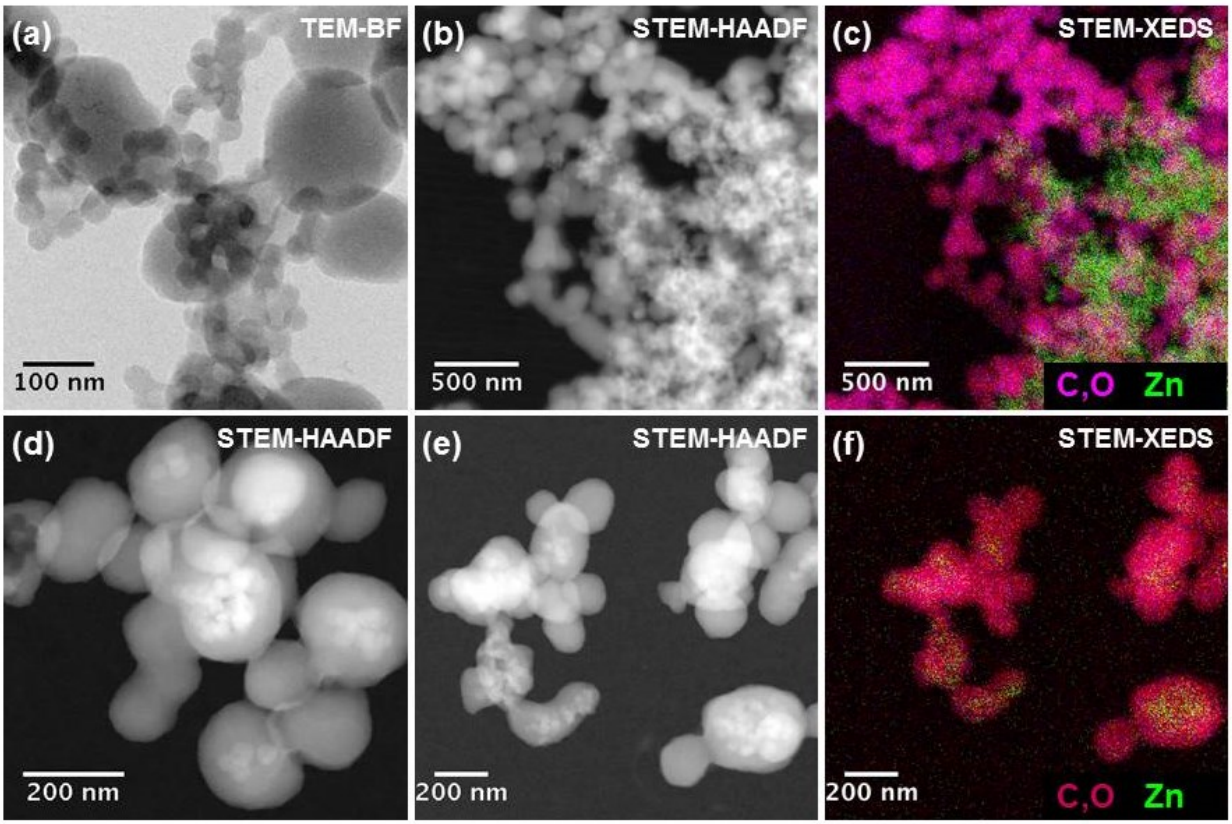

Figure 4 :TEM, STEM-HAADF and STEM-XEDS observations of ZIF-8/PIM-1 colloidal suspensions at ZIF-8/PIM-1 = 20/80 wt% with different ZIF-8 concentrations (a-c): [ZIF-8] = 0.1 $g.L^{-1}$; (d-f) : [ZIF-8] = 1 $g.L^{-1}$. For (d-f), TEM observations are performed on solutions that were ultra-sonicated before casting.

However, for a few aggregates, it seems that the polymer is also incorporated inside the structure of the aggregates. Indeed, one can observe that a few ZIF-8 NPs are screened by a polymer layer and their packing density is lower than that of pristine ZIF-8 NPs (see Figure 5).

By decreasing the polymer content to 70 and 50 wt% (i.e. ZIF-8/PIM-1 weight ratio equal to 30/70 and 50/50), similar compact aggregates of ZIF-8 NPs were observed with a 3 nm thick polymer shell at the surface. Therefore, the microstructure of ZIF-8 NPs is not affected by the polymer content in the range 50-80 wt%. For a few samples, it is remarkable that some local defects with size in the range 2-4 nm, are actually present at the surface of these objects (see Figure 5(a-d)). These defects possibly correspond to an incomplete coverage of the ZIF-8 NPs by the polymer, creating some holes in the polymer coating.

In order to enhance the colloidal stability of ZIF-8/PIM-1 suspensions, a short ultra-sonication step (1 min, 10 %) was applied. Whatever the ZIF-8/PIM-1 weight ratios (i.e. 50/50, 30/70, 20/80) and the ZIF-8 concentration (i. e. 0.1 or 1 g. L^{-1}), a significant decrease of the particle size can be observed since a single population of particle with D_h = 250±50 nm was detected. This is in a relative good agreement with STEM-HAADF observations, showing a distribution of ZIF-8 aggregates with diameters lower than 200 nm (see Figures 4(d)-(f) and Figure S14(b)). Moreover, STEM-HAADF images show that the samples contain not only independent ZIF-8 NPs and PIM-1 particles but also PIM-1 particles in which a few ZIF-8 NPs are encapsulated (see Figure 4(d)-(f) and Figure S15). The accommodation of ZIF-8 NPs inside PIM-1 particles was confirmed using elemental mapping via STEM-HAADF and STEM-XEDS analyses (see Figure 4 (f)). These results show that the ultra-sonication treatment of ZIF-8/PIM-1 solutions not only enhances the colloidal stability of the solutions but also the compatibility between the polymer and ZIF-8 NPs. Sonication has been widely used for the synthesis and/or dispersion of a wide range of organic and inorganic particles or filaments at the nano- or mesoscale. [53,54,55] It was also implemented for the functionalization of materials[56] and the formulation of nanoemulsions.[57] Most sonochemical effects are attributed to cavitation, namely the growth and rapid collapse of microscopic bubbles after applying a longitudinal sound wave to the solution. The principal origin of the enhanced

dispersion is the ultrahigh shear rate attained during cavitation events. As reported previously for the dispersion and/or length reduction of carbon nanotubes, silver nanowires or protein fibrils under ultrasonication,[58] it may be expected that the cohesive forces (i.e. hydrogen bonds, attractive van der Waals interactions) between PIM-1 chains inside the spherical aggregates are partially broken by the shear energy and/or eventually the local increase of temperature. Since a very short time of ultrasonication (~1 min) was applied to ZIF-8/PIM-1 mixtures, the destabilization of PIM-1 aggregates is limited but this may lead to a local increase of the PIM-1 concentration in THF and favor the interactions between PIM-1 macromolecules and ZIF-8 NPs. This phenomenon may explain why a few ZIF-8 NPs are integrated in the structure of PIM-1 particles under ultrasonication conditions while PIM-1 and ZIF-8 NPs are arranged in two independent networks of particles in the absence of ultrasonication treatment.

The impact of the polymer content on the colloidal stability of ZIF-8/PIM-1 solutions was investigated by DLS (Figure 6). This study was performed on non-sonicated solutions at ZIF-8 concentrations of 0.1 and 1 $g.L^{-1}$. Two opposite trends were observed depending on the ZIF-8 concentration. At [ZIF-8] = 1 $g\ L^{-1}$, by increasing the PIM-1 content from 0 to 80 wt%, a decrease of the diameter of aggregates from 3000 to 250 nm was observed, suggesting a stabilizing effect of the PIM-1 chains on ZIF-8/PIM-1 colloids. It is notable that pure ZIF-8 NPs are strongly aggregated at this concentration and the addition of polymer to the solution may induce the formation of ZIF-8/PIM-1 interactions at the expense of inter-particle interactions between ZIF-8 NPs. In contrast, at [ZIF-8] = 0.1 $g\ L^{-1}$, solutions of pure ZIF-8 NPs are significantly less aggregated than those at [ZIF-8] = 1 $g\ L^{-1}$ since particles of D_h = 200 nm are detected. By increasing the amount of polymer to 80 wt%, an increase of the diameter of particles to 500 nm is observed, suggesting that the polymer plays a role in enhancing aggregate formation presumably with the ZIF-8 NPs acting as cross-linking agents between different PIM-1 chains.

The impact of the molecular structure of the polymer on the compatibility with the ZIF-8 NPs was also investigated by using the PIM-EA-TB polymer (see Scheme 1). Similar results were obtained with the ZIF-8/PIM-EA-TB system for a ZIF-8 content ranging from 50, 30, and 20 wt%, showing the co-existence of PIM-EA-TB particles and compact aggregates of ZIF-8 NPs with a diameter of a few hundreds of nanometers (see Figure S16). Similarly to ZIF-8/PIM-1 particles, a 3 nm thick polymer layer is present at the surface of ZIF-8/ PIM-EA-TB aggregates and the ZIF-8 NPs are also screened by the polymer (see Figure S16 (e, f)). It is noticible that the density of the local defects in the PIM-EA-TB shell is significantly higher than that observed in ZIF-8/PIM-1 aggregates for similar polymer contents. However, the aggregation state of ZIF-8/ PIM-EA-TB is significantly different from that of ZIF-8/PIM-1 since it was not possible to obtain a stable colloidal solution by varying the different physico-chemical parameters (ultra-sonication, time of mixing, ZIF-8/PIM-EA-TB weight ratios). This may be explained by the poor solubility of PIM-EA-TB in THF and thus the need to use a mixture of solvents ($CHCl_3$ and THF) in order to solubilize both polymer and ZIF-8 NPs. Moreover, a lack of specific and strong interactions at the interface between ZIF-8 NPs and PIM-EA-TB may also hinder stable colloidal solutions.

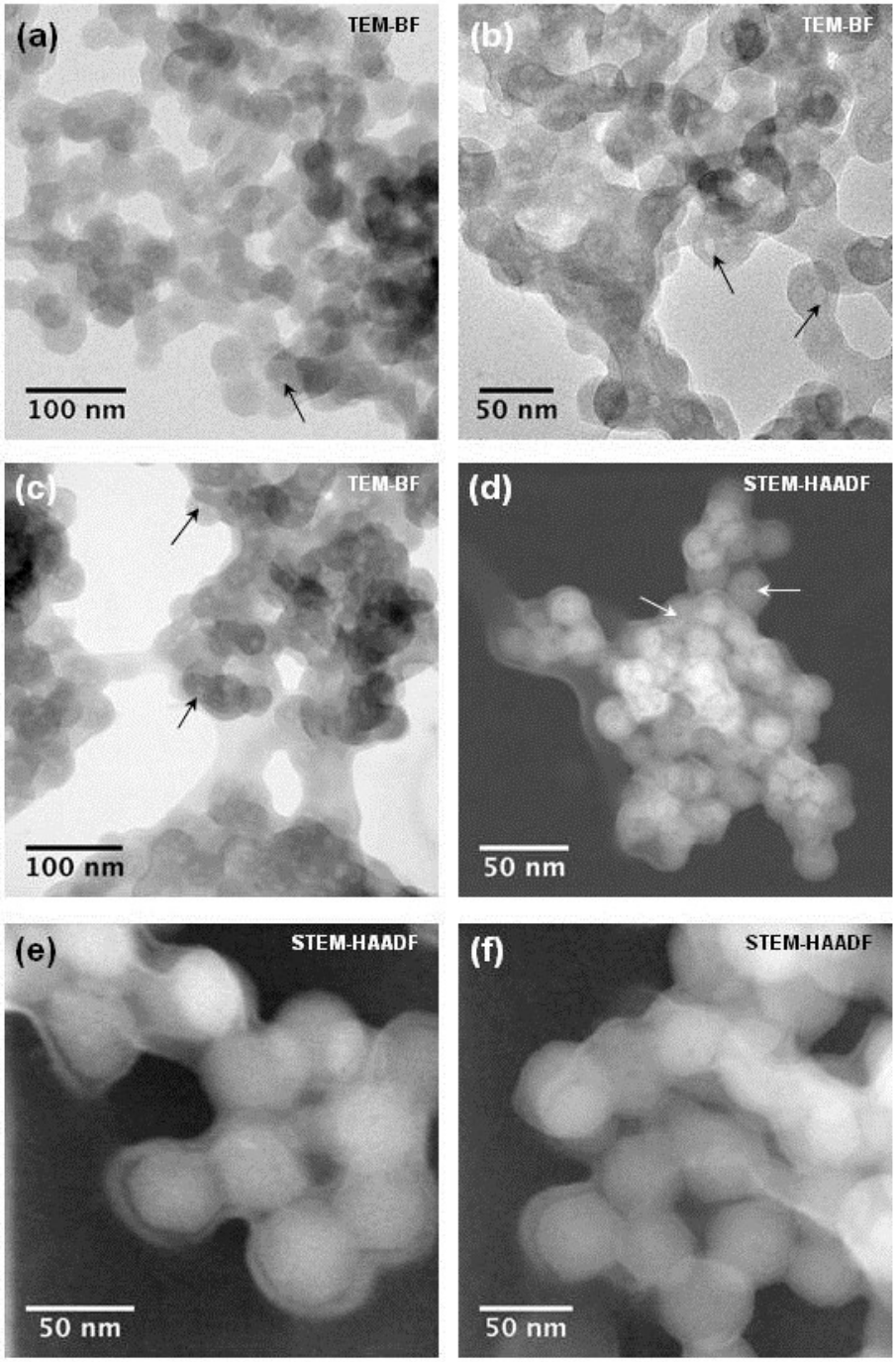

Figure 5. TEM bright field and STEM-HAADF images of ZIF-8/ PIM-1 colloidal suspensions at [ZIF-8] = 0.1 $g.L^{-1}$ with different ZIF-8/PIM-1 weight ratios: (a) 50/50; (b-d) 30/70; (e-f) 20/80. For the preparation of these solutions, the excess of polymer was removed by centrifugation at 14500 rpm for 15 min. Some defects are indicated by black and white arrows in the images.

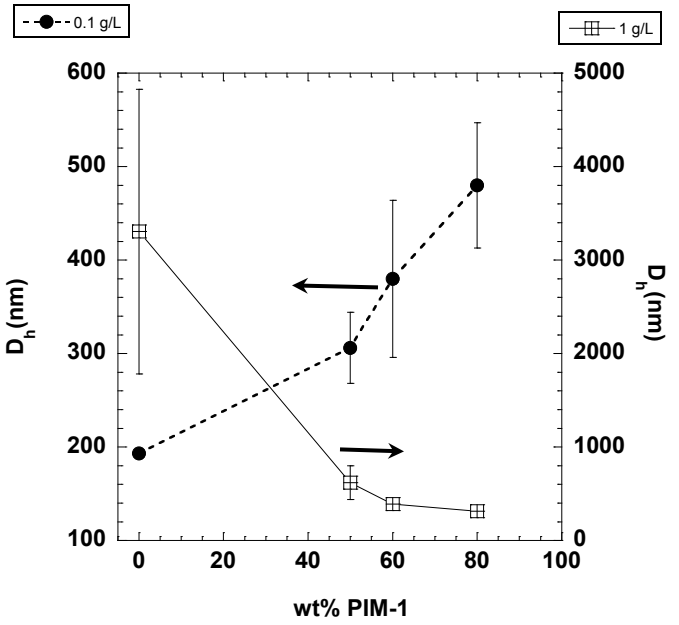

Figure 6. Evolution of the average hydrodynamic diameter of particles measured by DLS as a function of the PIM-1 content (wt%) for ZIF-8 concentrations of 0.1 g L^{-1} and 1 g L^{-1}

Characterization of ZIF-8/PIM-1 solutions by combining DLS and SAXS.

The dispersion of ZIF-8 with PIM-1 at different weight ratios leads to macroscopically homogeneous samples for [ZIF-8] = 0.01 g.L^{-1}. These samples were studied by SAXS as shown in Figure 7. It is notable that all the curves superimpose over the whole q range whatever the concentration of PIM-1, whose contribution to the scattering is negligible in THF relative to ZIF-8 as shown in Table S1 of the SI. At low q (i.e. $q \leq 0.01$ $Å^{-1}$), a power law decay of the scattered intensity, $I \alpha q^{-2.9}$, can be observed and at high q (i.e. $q > 0.01$ $Å^{-1}$), the SAXS pattern can be superimposed on the form factor of ZIF-8 previously measured at the same concentration (Figure S6 of SI). This indicates that ZIF-8 NPs form compact clusters (fractal dimension $D_f \approx 2.9$) in the presence of PIM-1 whatever the ZIF-8/PIM-1 weight ratio without precipitation. The size of the clusters is greater than 100 nm but cannot be determined in the available q-range.

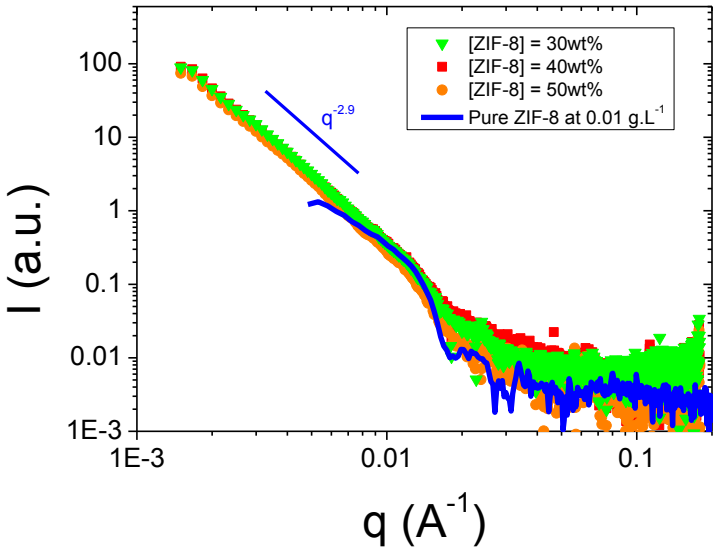

Figure 7. SAXS curves of ZIF-8/PIM-1 mixtures prepared four hours before the measurements at different ZIF-8 contents as indicated on the plot for a fixed concentration of ZIF-8: [ZIF-8] = 0.01 g L^{-1}. The blue line corresponds to the form factor of ZIF-8 measured at the same concentration as in Figure S6 of SI.

The dispersion of ZIF-8 (at 1 g L^{-1}) with PIM-1 at different weight ratios was studied by SAXS (Figure 8). At low q (i.e. $q \leq 0.01$ $Å^{-1}$), a power law decay of the scattered intensity, $I \propto q^{-2.5}$, can be observed and at high q (i.e. $q > 0.01$ $Å^{-1}$), the scattering pattern corresponds to the form factor of ZIF-8 with a characteristic oscillation at $q = 0.021$ $Å^{-1}$. Although, the curves obtained at different weight ratios depict the same evolution, they are clearly shifted in intensity. Thus, in contrast with the measurements performed at [ZIF-8] = 0.01 g.L^{-1} (Figure 7), no curve can be superimposed on the form factor of ZIF-8 corrected by the dilution effect. Instead, all the curves present lower intensities than that of ZIF-8 with a shift factor decreasing with ZIF-8/PIMs weight ratio which is in agreement with DLS measurements. Together these results indicate that ZIF-8 form clusters that phase separate in the presence of PIM-1 whatever the ZIF-8/PIMs molar ratio. These clusters are less compact than those obtained at lower ZIF-

8 concentration. The size of clusters is higher than 100 nm but cannot be determined in the available q-range. All these observations are consistent with previous TEM observations (Figure 4(d-f)).

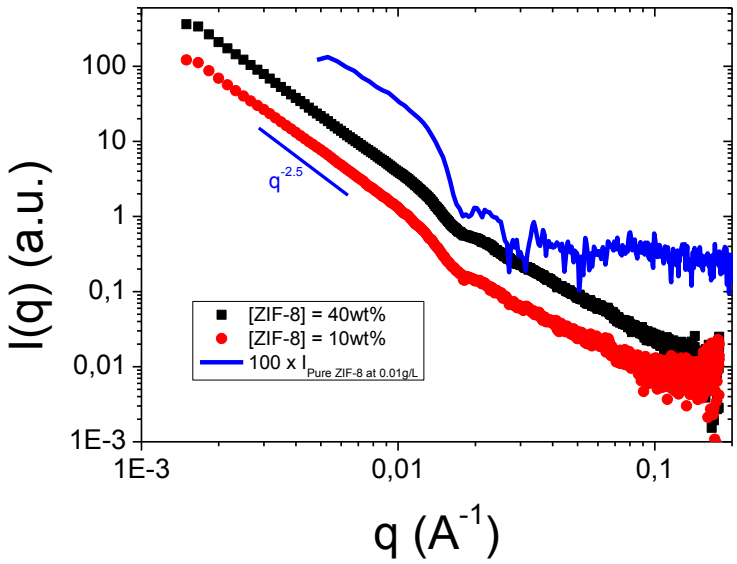

Figure 8. SAXS curves of ZIF-8/PIMs mixtures prepared four hours before the measurements at different ZIF-8 contents as indicated on the plot for a fixed concentration of ZIF-8: [ZIF-8] = 1 $g.L^{-1}$. The blue line corresponds to the form factor of ZIF-8 shifted by a factor 100 in intensity to compensate the factor of dilution.

Molecular Modeling of ZIF-8/PIMs interfacial structures.

The interfacial structure of the ZIF-8/PIM-EA-TB composite was further analyzed in order to provide a molecular-scale explanation for the interactions between the two components. Based on our previous findings for ZIF-8/PIM-1, the OH and NH terminal groups at the ZIF-8 surface could be thought to exhibit a predominant interaction with the N atoms of PIM-EA-TB. Radial distribution functions (RDFs) for different MOF surface terminations / polymer pairs, namely $(NH)_{ZIF\text{-}8}$ … $X_{PIM\text{-}EA\text{-}TB}$ and $(OH)_{ZIF\text{-}8}$ … $X_{PIM\text{-}EA\text{-}TB}$, were computed in order to interrogate this assumption. The corresponding data are summarized in Figure 9 and Figure S18.

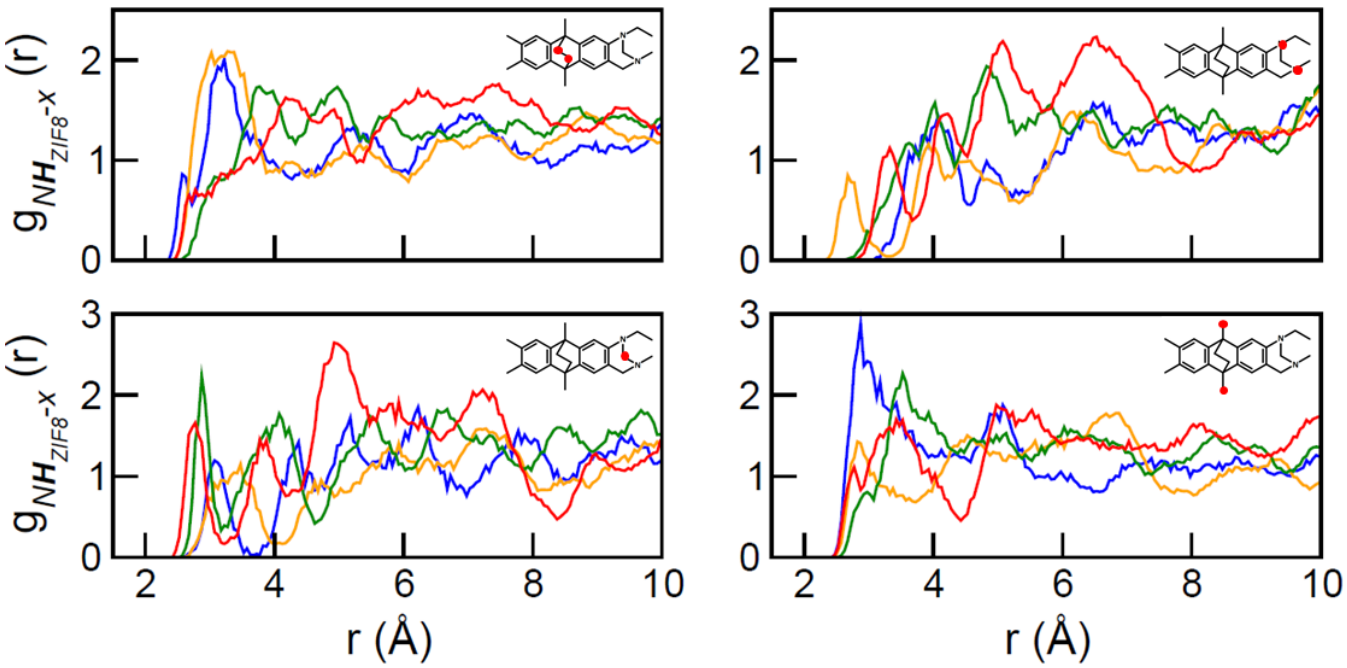

Figure 9. Radial distribution functions for the ZIF-8/PIM-EA-TB interface model, for the pairs $(NH)_{ZIF\text{-}8}$ … $X_{PIM\text{-}EA\text{-}TB}$. Results obtained from four different MD runs. $X_{PIM\text{-}EA\text{-}TB}$ sites are indicated in red in the inset scheme for each panel.

This collection of RDFs for PIM-EA-TB/ZIF-8 shows a similar trend with characteristic polymer/MOF distances of about 3.0 Å. Indeed, all polymer atoms seem to have, in average, very similar interactions with the surface groups of the MOF. This situation differs with what has been seen for the ZIF-8/PIM-1 composite, where a predominant interaction between the CN group of PIM-1 and the NH group of ZIF-8 was apparent[42] (see Figure S19). This difference can be ascribed to the fact that the N atoms in PIM-EA-TB are part of the fused-ring system of the polymer, and thus they are geometrically less exposed than the CN group of PIM-1 to interact with the MOF surface atoms. Moreover, as PIM-EA-TB exhibits a higher rigidity than PIM-1,[5] it may be less able to adapt its conformation to optimize interactions with the MOF surface.

In addition, the free volume distribution at the ZIF-8/PIM-EA-TB interface has been analyzed. Figure 10(a) shows the density of MOF and polymer atoms as a function of the *z*-coordinate, which corresponds to the direction perpendicular to the interface.

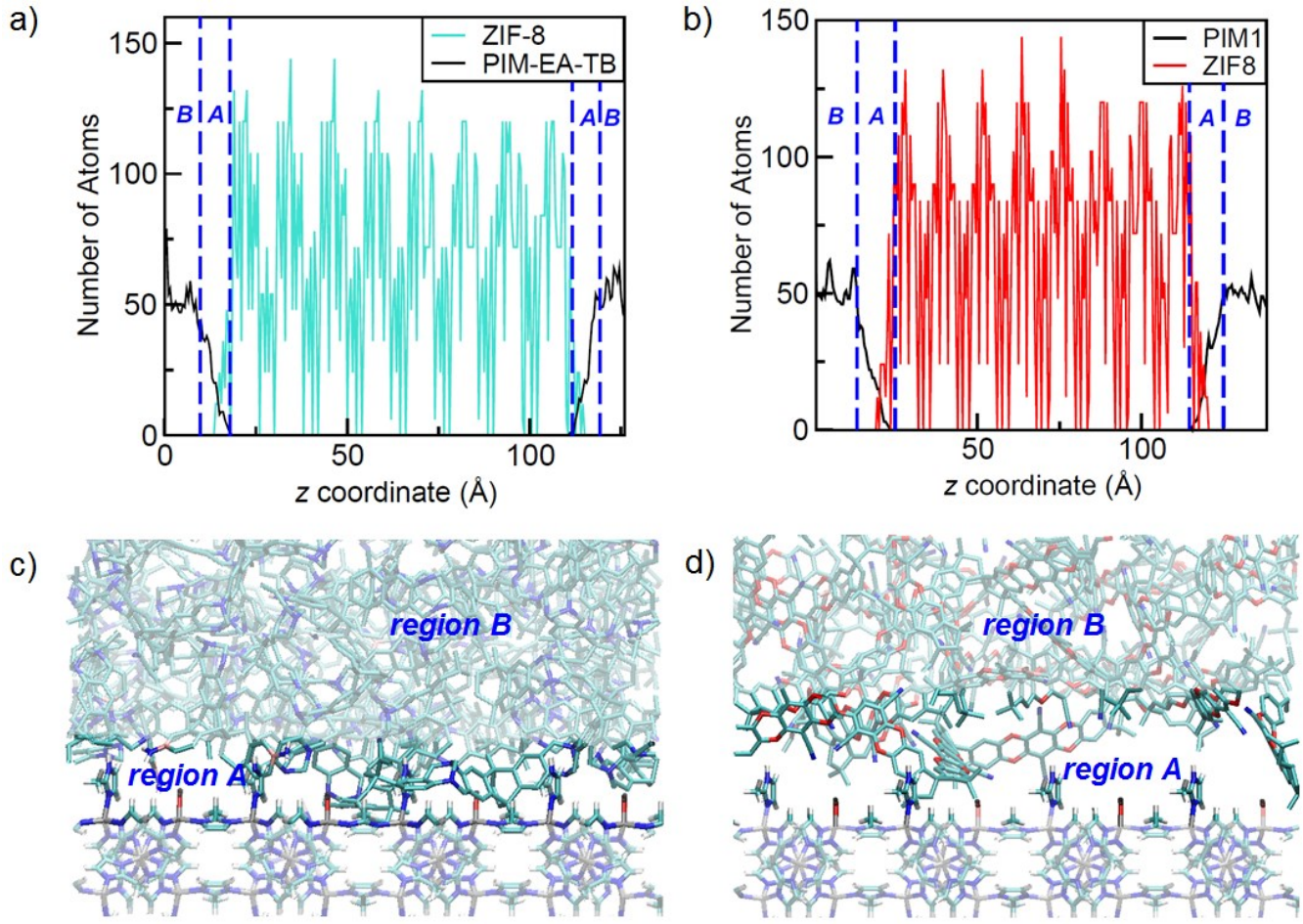

Figure 10. (a) Density of ZIF-8 and PIM-EA-TB atoms as a function of the *z*-coordinate for a representative configuration of ZIF-8/ PIM-EA-TB system. The blue dashed lines indicate the limits of ***regions A*** and ***B***. (b) Same plots for ZIF-8/ PIM-1 system (Figure 8 in [42]), (c) and (d) snapshots of ZIF-8/PIM-EA-TB and ZIF-8/PIM-1 interfaces respectively.

This profile is reminiscent to the one obtained for the ZIF-8/PIM-1 composite (Figure 10 b). On moving away from the ZIF-8 surface (z = 0), the number of polymer atoms varies from zero to an almost constant value in a linear-like fashion, so that two regions can be also distinguished in this case: ***region A*** and ***region B***. The former corresponds to the progressive growth in polymer density, while for the

latter the density oscillates around a constant value. The main difference between the two polymers in this aspect is that the z-length of ***region A*** is smaller for the PIM-EA-TB composite than for the PIM-1 composite, (9 ±1) Å versus (13 ± 2) Å (obtained from averaged values of 10 MD runs where the errors were computed by taking into account the standard deviation of the values). The maximum equivalent radii for the "interfacial microvoids" are comparable for PIM-EA-TB and PIM-1 composites, (5.3 ± 0.5) Å and (6.3 ± 0.5) Å respectively, which corresponds roughly to (11 ± 1) and (13 ± 1) Å in pore size (see Figure S20). The voids in ***region B*** are also of comparable size for the two polymers, (4.8 ± 0.6) Å versus (3.8 ±0.6) Å in radius. These values are similar to those reported from Positron Annihilation Lifetime Spectroscopy (PALS) measurements, R_3/R_4 = 2.52 Å/5.07 Å and 2.97 Å/5.11 Å for pure PIM-EA-TB and PIM-1 respectively.[43] This indicates that the influence of the MOF is rather limited at ~ 15-20 Å from the surface, as found for the ZIF-8/ PIM-1 system.[42]

These results suggest that the relatively moderate compatibility between ZIF-8 and the two polymers can be explained differently for each polymer on a molecular-scale. While PIM-1 mainly interacts with anchoring sites at the MOF surface, the composite involving PIM-EA-TB appears to be stabilized by a more homogeneous set of interactions (see Figure 10 (c,d)). However, in both cases micro-voids preclude an optimal adhesion of the two components at the interface. This is consistent with the experimental observation of ZIF-8 aggregates and the phase separation of PIMs resulting from a rather low affinity between the MOF and polymers.

■ CONCLUSIONS AND OUTLOOKS

This study used a combination of multimodal experimental and computational methods to investigate the complex microstructure of ZIF-8/PIMs membranes, which were found to consist mainly of two kinds of aggregates. Firstly, core-shell aggregates of a few 100 nm in diameter with a core composed of densely packed ZIF-8 NPs and a polymer shell of about 3 nm were observed by combining STEM-HAADF and HRTEM on ZIF-8/PIMs colloidal suspensions. Secondly, polymer aggregates of about

200 nm are also present, revealing a phase separation process for both polymers (i. e. PIM-1 and PIM-EA-TB) in THF and $CHCl_3$. By varying different physico-chemical parameters (i. e. concentration of ZIF-8, ZIF-8/PIMs weight ratio, time of mixing, ultra-sonication) for the processing of MMMs, it appears that the ultra-sonication step and the polymer content of the membranes significantly impact the size and stability of ZIF-8/PIM colloids. The presence of a polymer coating at the surface of the ZIF-8/PIM aggregates and the evolution of the size of ZIF-8/PIM-1 aggregates as a function of PIM-1 concentration are both in agreement with a moderate affinity of ZIF-8 for PIM-1 and PIM-EA-TB. For ZIF-8/PIM-1, the molecular simulations reveal that there is a preferential interaction between the CN group of PIM-1 and the NH groups of the imidazole moieties at the MOF surface, while for ZIF-8/PIM-EA-TB, the interactions are more uniform with none stronger than the others. However, for both polymers the microscopic coverage is far from being homogeneous, with the presence of "interfacial microvoids" apparent. As a result, there are zones at the interface where the polymer backbone lays at long distance with respect to the ZIF-8 surface, weakening the interactions between both components. This suggests that the PIM/ZIF-8 interactions may not be high enough to overcome the self-aggregation of ZIF-8 NP and the phase separation of PIMs. These results emphasize the important role of the organic solvent for processing MMMs. As reported previously,[11,43] the microstructure of PIM-based MMMs is strongly dependent on the non-solvents used for the post-processing conditioning of membranes. In particular, the treatment of MMMs with non-solvents can induce a swelling of PIMs that may affect the free pore volume of the polymers and thus their gas transport properties.[7] Herein, we show that solvents such as THF and $CHCl_3$ not only influence the surface area and pore volume of PIMs but also their self-assembly behavior in solution. Moreover, the strong clustering of ZIF-8 NPs in these solvents is another limiting parameter for the processing of highly homogeneous MMMs. This work is in line with the need to process MMMs following novel approaches with the aim of enhancing the compatibility between MOF filler and polymer. The introduction of co-solvent or co-polymers as compatibilizing agents, the use of surface modified MOF NPs or MOFs containing an organic linker

structurally similar to one monomer of the polymer, are potential strategies to improve the interfacial properties of MMMs. [22,37,59,60]

■ ASSOCIATED CONTENT

Supporting Information. Additional figures and tables; XRPD, TGA, N_2 sorption isotherm, SEM TEM, DLS and SAXS of ZIF-8 NPs; DLS of PIM-1 and PIM-EA-TB solutions; XRPD, FT-IR, ^{13}C CP MAS of ZIF-8/PIM-1 MMMs; SEM, elemental mapping and cross-section image SEM of ZIF-8/PIM-1 membranes (ZIF-8/PIM-1 = 10/90 wt%); SEM and elemental mapping of ZIF-8/PIM-1 membranes (ZIF-8/PIM-1 = 20/80 wt%); HAADF-STEM images of ZIF-8/PIM-1 solutions at ZIF-8/PIM-1 = 20/80 wt%; TEM and HAADF-STEM images of ZIF-8/PIM-EA-TB colloidal suspensions; Scheme of PIM-EA-TB polymer; Atom types, charges and Lennard-Jones parameters for the PIM-EA-TB model; Radial distribution functions for the ZIF-8/PIM-1 and ZIF-8/PIM-EA-TB interface models; Pore number and free volume of the pores as a function of their radius computed for ZIF-8/PIM-EA-TB.

This information is available free of charge via the Internet at http://pubs.acs.org/.

■ AUTHOR INFORMATION

Corresponding author

nathalie.steunou@uvsq.fr; Fax : ++33 1 39 25 44 52

■ ACKNOWLEDGMENT

The authors would like to acknowledge the European Community Seventh Program (FP7/2007-2013) for funding the research presented in this article under Grant Agreement No. 608490 (project M4CO2). The authors acknowledge synchrotron SOLEIL for SAXS beam time allocation and Thomas Bizien (SWING, SOLEIL, Saint-Aubin, France) for his help during SAXS experiments. The authors acknowledge Charlotte Martineau (ILV, Versailles) for recording ^{13}CP MAS experiments and Aziz Ghoufi (Université Rennes 1) for fruitful discussions. G.M. thanks Institut Universitaire de France for its support.

REFERENCES

[1] Moulijn, J. A.; Makkee, M.; van Diepen, A. *Chemical Process Technology*; John Wiley & Sons: Chichester, England, 2001.

[2] Robeson, L. M. Correlation of Separation Factor Versus Permeability for Polymeric Membranes, *J. Membr. Sci.* **1991**,*62*, 165-185.

[3] Robeson, L. M. The Upper Bound Revisited. *J. Membr. Sci.* **2008**, *320*, 390-400.

[4] Carta, M.; Malpass-Evans, R.; Croad, M.; Rogan, Y.; Jansen, J. C.; Bernardo, P.; Bazzarelli, F.; McKeown, N. B. An Efficient Polymer Molecular Sieve for Membrane Gas Separations. *Science* **2013**, *339*, 303-307.

[5] Guiver, M. D.; Lee, Y. M. Polymer Rigidity Improves Microporous Membranes. *Science* **2013**, *339*, 284-285.

[6] Budd, P. M.; Msayib, K. J.; Tattershall, C. E.; Ghanem, B. S.; Reynolds, K. J.; McKeown, N. B.; Fritsch, D. Gas Separation Membranes from Polymers of Intrinsic Microporosity. *J. Membr. Sci.* **2005**, *251*, 263-269.

[7] Budd, P. M.; McKeown, N. B.; Ghanem, B. S.; Msayib, K. J.; Fritsch, D.; Starannikova, L.; Belov, N.; Sanfirova, O.; Yampolskii, Y.; Shantarovich, V. Gas Permeation Parameters and other Physicochemical Properties of a polymer of Intrinsic Microporosity: Polybenzodioxane PIM-1. *J. Membr. Sci.* **2008**, *325*, 851-860.

[8] Du, N.; Park, H. B.; Robertson, G. P.; Dal-Cin, M. M.; Visser, T.; Scoles, L.; Guiver, M. D. Polymer Nanosieve Membranes for CO_2-Capture Applications. *Nat. Mater.* **2011**, *10*, 372-375.

[9] Budd, P. M. ; Elabas, E. S. Ghanem, B. S.; Makhseed, S.; McKeown, N. B.; Msayib, K. J.; Tattershall, C. E.; Wang, D. Solution-Processed, Organophilic Membrane Derived from a Polymer of Intrinsic Microporosity. *Adv. Mater.* **2004**, *16*, 456-459.

[10] Hill, A. J.; Pas, S. J.; Bastow, T. J.; Burgar, M. I.; Nagai, K.; Toy, L. G.; Freeman, B. D. Influence of Methanol Conditioning and Physical Aging on Carbon Spin-Lattice Relaxation Times of poly(1-trimethylsilyl-1-propyne). *J. Membr. Sci.* **2004**, *243*, 37−44.

[11] Jue, M. L.; McKay, C. S.; McCool, B. A.; Finn, M. G.; Lively, R. P. Effect of Nonsolvent Treatments on the Microstructure of PIM-1. *Macromolecules* **2015**, *48*, 5780-5790.

[12] Yampolskii, Y.; Alentiev, A.; Bondarenko, G.; Kostina, Y.; Heuchel, M. Intermolecular Interactions : New Way to Govern Transport Properties of Membrane Materials. *Ind. Eng. Chem. Res.* **2010**, *49*, 12031-12037.

[13] Zornoza, B.; Tellez, C.; Coronas, J.; Gascon, J.; Kapteijn, F. Metal Organic Framework based Mixed Matrix Membranes: An Increasingly Important Field of Research with a Large Application Potential. *Microporous Mesoporous Mater.* **2013**, *166*, 67–78.

[14] Qiu, S.; Xue, M.; Zhu, G. Metal–Organic Framework Membranes: from Synthesis to Separation Application. *Chem. Soc. Rev.* **2014**, *43*, 6116-6140.

[15] Matteucci, S.; Kusuma, V. A.; Sanders, D.; Swinnea, S.; Freeman, B. D. Gas Transport in TiO_2 Nanoparticle-filled Poly(1-trimethylsilyl-1-propyne). *J. Membr. Sci.* **2008**, *307*, 196–217.

[16] Ahn, J. ; Chung, W.-J. ; Pinnau, I.; Song, J.; Du, N.; Robertson, G. P. ; Guiver, M. D. Gas Transport Behavior of Mixed-Matrix Membranes Composed of Silica Nanoparticles in a Polymer of Intrinsic Microporosity (PIM-1). *J. Membr. Sci.* **2010**, *346*, 280-287.

[17] Roh, D. K.; Kim, S. J.; Jeon, H.; Kim, J. H. Nanocomposites with Graft Copolymer-Templated Mesoporous $MgTiO_3$ Perovskite for CO Capture Applications. *ACS Appl. Mater. Interfaces*, **2013**, *5*, 6615–6621.

[18] Rangnekar, N. ; Mittal, N. ; Elyassi, B. ; Caro, J. ; Tsapatsis, M. Zeolite Membranes – a Review and Comparison with MOFs. *Chem. Soc. Rev.* **2015**, *44*, 7128-7154.

[19] Laghaei, M. ; Sadeghi, M. ; Ghalei, B. ; Shahrooz, B. The Role of Compatibility Between Polymeric Matrix and Silane Coupling Agents on the Performance of Mixed Matrix Membranes: Polyethersulfone/MCM-41. *J. Membr. Sci.* **2016**, *513*, 20–32.

[20] Rodenas, T.; Luz, I.; Prieto, G.; Seoane, B.; Miro, H.; Corma, A.; Kapteijn, F.; Llabrés I Xamena, F. X.; Gascon, J. Metal-Organic Framework Nanosheets in Polymer Composite Materials for Gas Separation. *Nat. Mater.* **2015**, *14*, 48-55.

[21] Su, N. C.; Sun, D. T.; Beavers, C. M.; Britt, D. K.; Queen, W. L.; Urban, J. J. Enhanced Permeation Arising from Dual Transport Pathways in Hybrid Polymer-MOF Membranes. *Energy. Environ. Sci.* **2016**, *9*, 922-931.

[22] Denny, Jr. M. S.; Cohen, S. M. In Situ Modification of Metal–Organic Frameworks in Mixed-Matrix Membranes. *Angew. Chem. Int. Ed.* **2015**, *54*, 9029 –9032.

[23] Seoane, B.; Coronas, J.; Gascon, I.; Benavides, M. E.; Karvan, O.; Caro, J.; Kapteijn, F.; Gascon, J. Metal–Organic Framework based Mixed Matrix Membranes: a Solution for Highly Efficient CO_2 Capture? *Chem. Soc. Rev.* **2015**, *44*, 2421-2454.

[24] Zhang, Z.; Hoang Nguyen, H. T.; Miller, S. A.; Ploskonka, A. M.; DeCoste, J. B.; Cohen, S. M. Polymer-Metal-Organic Frameworks (polyMOFs) as Water Tolerant Materials for Selective Carbon Dioxide Separations. *J. Am. Chem. Soc.* **2016**, *138*, 920-925.

[25] Belmabkhout, Y.; Guillerm,V.; Eddaoudi, M. Low Concentration CO_2 Capture using Physical Adsorbents: Are Metal–Organic Frameworks Becoming the New Benchmark Materials? *Chem. Eng. J.* **2016**, *296*, 386–397.

[26] Sumida, K.; Moitra, N.; Reboul, J.; Fukumoto, S.; Nakanishi, K.; Kanamori, K.; Furukawa, S.; Kitagawa, S. Mesoscopic Superstructures of Flexible Porous Coordination Polymers Synthesized via Coordination Replication. *Chem. Sci.* **2015**, *6*, 5938–5946.

[27] Smith, S. J. D.; Ladewig, B. P.; Hill, A. J.; Lau, C. H.; Hill, M. R. Post-Synthetic Ti Exchanged UIO-66 Metal-Organic Frameworks that deliver Exceptional Gas Permeability in Mixed Matrix Membranes. *Sci. Rep.* **2015**, *5*, 7823.

[28] Dai, Y.; Johnson, J. R.; Karvan, O.; Sholl, D. S. ; Koros, W. J. Ultem®/ZIF-8 Mixed Matrix Hollow Fiber Membranes for CO_2/N_2 Separations. *J. Membr. Sci.* **2012**, *401-402*, 76-82.

[29] Shahid, S.; Nijmeijer, K.; Nehache, S.; Vankelecom, I.; Deratani, A.; Quemener, D. MOF-Mixed Matrix Membranes: Precise Dispersion of MOF Particles with Better Compatibility via a Particle Fusion Approach for Enhanced Gas Separation Properties. *J. Membr. Sci.* **2015**, *492*, 21–31.

[30] Perez, E.V.; Balkus Jr., K. J.; Ferraris, J. P.; Musselman, I. H. Mixed-Matrix Membranes Containing MOF-5 for Gas Separations, *J. Membr. Sci.* **2009**, *328*, 165–173.

[31] Ordonez, M. J. C.; Balkus Jr, K. J.; Ferraris, J. P.; Musselman, I. H.; Molecular Sieving Realized with ZIF-8/Matrimid(R) Mixed-Matrix Membranes, *J. Membr. Sci.* **2010**, *361*, 28–37.

[32] Song, Q.; Nataraj, S. K.; Roussenova, M. V.; Tan, J. C.; Hughes, D. J.; Li, W.; Bourgoin, P.; Alam, M. A.; Cheetham, A. K.; Al-Muhtaseb, S. A.; Sivaniah, E.; Zeolitic Imidazolate Framework (ZIF-8) based Polymer Nanocomposite Membranes for Gas Separation, *Energy Environ. Sci.* **2012**, *5*, 8359–8369.

[33] Mahajan, R.; Koros, W. J. Mixed Matrix Membrane Materials with Glassy Polymers. Part. 1. *Polym. Eng. Sci.* **2002**, *42*, 1420-1431.

[34] Tien-Binh, N.; Vinh-Thang, H.; Chen, X. Y.; Rodrigue, D.; Kaliaguine, S. Polymer Functionalization to Enhance Interface Quality of Mixed Matrix Membranes for High CO_2/CH_4 Gas Separation. *J. Mater. Chem. A.* **2015**, *3*, 15202-15213.

[35] Rodenas, T.; van Dalen, M.; Garcia-Pérez, E.; Serra-Crespo, P.; Zornoza, B.; Kapteijn, F.; Gascon, J. Visualizing MOF Mixed Matrix Membranes at the Nanoscale : Towards Structure-Performance Relationships in CO_2/CH_4 Separation Over NH_2-MIL-53(Al)@PI. *Adv. Funct. Mater.* **2014**, *24*, 249-256.

[36] Guo, X.; Huang, H.; Ban, Y.; Yang, Q.; Xiao, Y.; Li, Y.; Yang, W.; Zhong, C. Mixed Matrix Membranes Incoporated with Amine-Functionalized Titanium-based Metal-Organic Framework for CO_2/CH_4 Separation. *J. Membr. Sci.* **2015**, *478*, 130–139.

[37] Wang, Z.; Wang, D.; Zhang, S.; Hu, L.; Jin, J. Interfacial Design of Mixed Matrix Membranes for Improved Gas Separation Performance. *Adv. Mater.* **2016**, *28*, 3399-3405.

[38] Bushell, A. F.; Attfield, M. P.; Mason, C. R.; Budd, P. M.; Yampolskii, Y.; Starannikova, L.; Rebrov, A.; Bazzarelli, F.; Bernardo, P.; Jansen, J. C.; Lanc, M.; Friess, K.; Shantarovich, V.; Gustov, V.; Isaeva, V. Gas Permeation Parameters of Mixed Matrix Membranes Based on the Polymer of Intrinsic Microporosity PIM-1 and the Zeolitic Imidazolate Framework ZIF-8. *J. Membr. Sci.* **2013**, *427*, 48–62.

[39] Banerjee, R.; Phan, A.; Wang, B.; Knobler, C.; Furukawa, H.; O'Keeffe, M.; Yaghi, O. M. High-Throughput Synthesis of Zeolitic Imidazolate Frameworks and Application to CO_2 Capture. *Science* **2008**, *319*, 939-943.

[40] Bux, H. ; Liang, F. ; Li, Y.; Cravillon, J.; Wiebcke, M.; Caro, J. Zeolitic Imidazolate Framework Membrane with Molecular Sieving Properties by Microwave-Assisted Solvothermal Synthesis. *J. Am. Chem. Soc.* **2009**, *131*, 16000-16001.

[41] Shekhah, O.; Swaidan, R.; Belmabkhout, Y.; du Plessis, M.; Jacobs, T.; Barbour, L. J.; Pinnau, I.; Eddaoudi, M. The Liquid Phase Epitaxy Approach for the Successful Construction of Ultra-Thin and Defect-free ZIF-8 Membranes: Pure and Mixed Gas Transport Study. *Chem. Commun.* **2014**, *50*, 2089-2092.

[42] Semino R.; Ramsahye, N. A.; Ghoufi, A.; Maurin G. Microscopic Model of the Metal-Organic Framework/Polymer Interface: A First Step toward Understanding the Compatibility in Mixed Matrix Membranes. *ACS Appl. Mater. Interfaces* **2016,** *8,* 809-819.

[43] Tocci, E.; De Lorenzo, L.; Bernardo, P. ; Clarizia, G. ; Bazzarelli, F. ; Mckeown, N. B. ; Carta, M. ; Malpass-Evans, R. ; Friess, K. ; Pilnacek, K.; Lanc, M.; Yampolskii, Y. P.; Strarannikova, L.; Shantarovich, V.; Mauri, M.; Jansen, J. C. Molecular Modeling and Gas Permeation Properties of a Polymer of Intrinsic Microporosity Composed of Ethanoanthracene and Tröger's Base Units. *Macromolecules* **2014**, *47*, 7900-7916.

[44] Cravillon, J.; Münzer, S. ; Lohmeier, S.-J. ; Feldhoff, A.; Huber, K.; Wiebcke, M. Rapid Room-Temperature Synthesis and Characterization of Nanocrystals of a Prototypical Zeolitic Imidazolate Framework.*Chem. Mater.* **2009**, *21*, 1410-1412.

[45] Cravillon, J.; Nayuk, R.; Springer, S.; Feldhoff, A.; Huber, K.; Wiebcke, M. Controlling Zeolitic Imidazolate Framework Nano- and Microcrystal Formation: Insight into Crystal Growth by Time Resolved In Situ Static Light Scattering. *Chem. Mater.* **2011**, *23*, 2130-2141.

[46]Abbott, L. J.; Hart, K. E.; Colina, C. M. Polymatic: A Generalized Simulated Polymerization Algorithm for Amorphous Polymers. *Theor. Chem. Acc.* **2013,** *132*, 1334.

[47] Eggimann, B. L.; Sunnarborg, A. J.; Stern, H. D.; Bliss, A. P.; Siepmann, J. I. An Online Parameter and Property Database for the TraPPe Force Field. *Mol. Simul.* **2014,** *40*, 101-105.

[48] Demessence, A.; Boissiere, C.; Grosso, D.; Horcajada, P.; Serre, C.; Ferey, G.; Soler-Illia, G. J. A. A.; Sanchez, C. Adsorption Properties in High Optical Quality NanoZIF-8 Thin Films with Tunable Thickness. *J. Mater. Chem.* **2010**, *20*, 7676–7681.

[49] Cravillon, J.; Schröder, C. A.; Nayuk, R.; Gummel, J.; Huber, K.; Wiebcke, M. Fast Nucleation and Growth of ZIF-8 Nanocrystals Monitored by Time Resolved In Situ Small-Angle and Wide-Angle X-Ray Scattering. *Angew. Chem. Int. Ed.* **2011**, *50*, 8067–8071.

[50] Chaukura, N.; Maynard-Atem, L. Interaction of a Polymer of Intrinsic Microporosiy (PIM-1) with Penetrants. *Am. J. Appl. Chem.* **2015**, *3*, 139-146.

[51] Knebel, A. ; Friebe, S. ; Bigall, N. C.; Benzaqui, M.; Serre, C.; Caro, J. Comparative Study of MIL-96(Al) as Continuous Metal-Organic Frameworks Layer and Mixed-Matrix Membrane. *ACS Appl. Mater. Interfaces* **2016,** *8*, 7536-7544.

[52] Nafisi, V.; Hägg, M. -B. Development of Dual Layer of ZIF-8/PEBAX-2533 Mixed Matrix Membrane for CO_2 Capture. *J. Membr. Sci.* **2014**, *459*, 244–255.

[53] Toumia, Y.; Domenici, F.; Orlanducci, S.; Mura, F.; Grishenkov, D.; Trochet, P.; Lacerenza, S.; Bordi, F.; Paradossi, G. Graphene Meets Microbubbles: A Superior Contrast Agent for Photoacoustic Imaging. *ACS Appl. Mater. Interfaces* **2016**, *8*, 16465−16475.

[54] Dong, H.; Tang, S.; Hao, Y.; Yu, H.; Dai, W.; Zhao, G.; Cao,Y.; Lu, H.; Zhang, X.; Ju, H. Fluorescent MoS2 Quantum Dots: Ultrasonic Preparation, Up- Conversion and Down-Conversion Bioimaging, and Photodynamic Therapy. *ACS Appl. Mater. Interfaces* **2016**, *8*, 3107−3114.

[55] Wang, X.; Wang, Q.; Wang, Q.; Gao, F.; Gao, F.; Yang, Y.; Guo, H. Highly Dispersible and Stable Copper Terephthalate Metal−Organic Framework−Graphene Oxide Nanocomposite for an Electrochemical Sensing Application. *ACS Appl. Mater. Interfaces* **2014**, *6*, 11573−11580.

[56] Borodina, T. N.; Grigoriev, D. O.; Carillo, M. A.; Hartmann, J.; Moehwald, H.; Shchukin, D. G. Preparation of Multifunctional Polysaccharide Microcontainers for Lipophilic Bioactive Agents. *ACS Appl. Mater. Interfaces* **2014**, *6*, 6570−6578.

[57] Periasamy, V. S.; Athinarayanan, J.; Alshatwi, A. A. Anticancer Activity of an Ultrasonic Nanoemulsion Formulation of Nigella sativa L. Essential Oil on Human Breast Cancer Cells. *Ultrason. Sonochem*. **2016**, *31*, 449–455.

[58] Huang, Y. Y.; Knowles, T. P. J. Terentjev, E. M. Strength of Nanotubes, Filaments, and Nanowires From Sonication-Induced Scission. *Adv. Mater.* **2009**, *21*, 3945–3948.

[59] Lin, R.; Ge, L.; Hou, L.; Strounina, E.; Rudolph, V.; Zhu, Z. Mixed Matrix Membranes with Strenghtened MOFs/Polymer Interfacial Interaction and Improved Membrane Performance. *ACS Appl. Mater. Interfaces* **2014**, *6*, 5609-5618.

[60] Anjum, M. W.; Vermoortele, F.; Khan, A. L.; Bueken, B.; De Vos, D. E.; Vankelecom, I. F. J. Modulated UiO-66-Based Mixed-Matrix Membranes for CO_2 Separation. *ACS Appl. Mater. Interfaces* **2015,** *7*, 25193−25201.

Table of Contents